J Mater Sci (2006) 41:5235–5241
DOI 10.1007/s10853-006-0588-4

Analytical electron microscope study of the dissolution of the Fe_3C iron carbide phase (cementite) during a graphitisation anneal of carbon steel

K. He · A. Brown · R. Brydson · D. V. Edmonds

Received: 16 May 2006 / Accepted: 31 May 2006 / Published online: 1 August 2006

Abstract The evolution of microstructure and composition of the Fe_3C iron carbide phase (cementite) during a graphitisation anneal of a quenched, medium carbon steel has been studied by analytical electron microscopy, including energy dispersive X-ray spectroscopy (EDX), electron energy loss spectroscopy (EELS) and energy filtered transmission electron microscopy (EFTEM) imaging. During heat treatment at 680 °C, dissolution of the cementite particles dispersed in the martensitic matrix was completed within a time period of 1.5 h, during which time graphite nodules began to form. However, a non-graphitic carbon-rich amorphous phase was also detected during this heat treatment. It is postulated that these amorphous particles could be an intermediate stage during the overall graphitisation process.

Introduction

The importance of Fe_3C iron carbide phase, or cementite, in steels is entirely due to its position as the major second phase constituent in a wide variety of commercial carbon and alloy steels, and as a consequence, its formation and effect on mechanical properties has been extensively studied and documented [1–5]. An example, related to the present work, is the formation and coarsening of Fe_3C during the various stages of tempering martensite in carbon steels: annealing at 600–700 °C would constitute the final coarsening stage of tempering. However, emphasis has mainly been placed upon this formation and coarsening of cementite, rather than upon its dissolution, although this transformation is quite relevant to the dispersal of carbon important to any subsequent stage of heat treatment: this might be heating to austenitise the steel, or in the present instance, prolongation of the period of annealing to graphitise the steel. In the case of graphitisation of conventional carbon steel compositions, this is expected to require long times, usually many tens or even hundreds of hours at temperature [6, 7]. However, in the present work the carbon steel has been alloyed to reduce graphitisation times. The present paper thus reports observations made of the cementite dissolution process as the precursor to graphitisation, in which essentially, a dispersion of coarsened cementite particles is exchanged for a dispersion of small graphite nodules. In this process the dissolution of the cementite assumes critical importance, as it is the source of carbon atoms for the nucleation and growth of the graphite.

In the present paper, the electron microscopic observations of the evolution of the microstructure, and the structure and composition of the cementite particles during annealing, including results obtained using electron energy loss spectroscopy (EELS) and energy filtered transmission electron microscopy (EFTEM), are reported. These latter techniques have not long been developed [8–14], and of relevance to the present study is their quite recent application to the examination of the graphitisation of carbonaceous precursor materials [15–20]. It has been demonstrated that information in the EELS spectra can be used to gain information on atomic coordination and

K. He · A. Brown · R. Brydson · D. V. Edmonds (✉)
Institute for Materials Research, University of Leeds, Leeds LS2 9JT, UK
e-mail: d.v.edmonds@leeds.ac.uk

electronic configuration: in the case of carbon this can be the average C–C bond length, the % sp^2 hybridisation C content, and the valence electronic density. Of late, analysis of the low loss ''plasmon'' region of the EELS spectrum, which arises from oscillation of the valence electron cloud, has been shown to be particularly useful in the study of carbon graphitisation [21, 22].

Experimental procedures

Compositions of the steels used are given in Table 1. High-purity elements were used to make 50 g ingots of steels A and B in an arc melting furnace under a partial pressure of argon gas. The argon-arc ingots were homogenised at 1,150 °C for 70 h and then water quenched. Steel C is a commercial 1053 steel, austenitised at 1,150 °C for 0.5 h and water quenched. Specimens cut from the quenched steels were annealed at 680 °C for various times. Samples for transmission electron microscopy (TEM) were first mechanically ground to a thickness of 80–100 μm from thin slices, followed by electropolishing at 20 mA, 15 V and ~ –10 °C, in a twin-jet unit using an electrolyte of 10% perchloric acid, 30% 2-butoxyethanol and 60% ethyl alcohol.

TEM examination and microanalysis were carried out either in a Philips CM 20, operating at 200 kV, with an Oxford ultra thin window EDX attachment and ISIS software, or a CM200 FEGTEM, fitted with a Schottky emitter source operated at 197 kV. For the latter equipment, in addition to energy dispersive X-ray analysis (EDX), EELS spectra and EFTEM images were recorded using a Gatan Imaging Filter 200. Processing was performed using Gatan Digital Micrograph and EL/p software. Core-loss EELS spectra were collected in selected area diffraction mode (image-coupled) with the effective diameter of the selected area being ~180 nm in the final image plane. To quantify the carbon content in the precipitates, 0.5 eV/pixel EELS spectra that contain both carbon K edge and iron $L_{2,3}$ edges were collected. Quantification was performed with both Hartree-Slater cross-sections and hydrogenic cross-sections (with a correction for the Fe $L_{2,3}$-white lines), with the following experimental parameters: beam energy 197 kV, convergence angle ~1 mrad, and collection angle 5.9 mrad.

Results

In the as-quenched samples from experimental steel A, only inclusion particles of aluminium nitride and aluminium oxide (in the approximate size range 0.3–3.0 μm in diameter) were observed in a martensitic matrix. After being annealed at 680 °C for 0.5 h, a dispersion of cementite particles, ranging from approximately 0.1 to 1.0 μm diameter with an average diameter of ~0.3 μm, was observed, mainly located at the remaining interfaces of ferrite (formerly martensite) laths or plates, along with a much lower density of graphite particles formed on the aluminium nitrides or oxides, as shown in Fig. 1. As the annealing time was increased to 1 h, most of these cementite particles disappeared and many more graphite nodules were formed, and after 1.5 h, no cementite particles remained and only graphite nodules were observed, but now in a more polygonal ferrite matrix (Fig. 2). In contrast, in the steels with higher concentrations of carbide stabilising elements, steels B and C, carbide was still present after many hours of annealing: the carbides shown in Fig. 3 are cementite containing Mn and/or Cr.

Examination by microanalytical TEM methods revealed unexpectedly that some of the particles observed in experimental steel A, with high Si and Al alloying, after the annealing treatments, and some portions of apparent cementite precipitates, did not have the structure and composition of cementite or graphite, nor were they oxide or nitride in nature. Many of the particles either surviving, or formed, after annealing for more than 0.75 h had a partly non-crystalline or amorphous structure. In a number of cases observed the particles were complex, consisting of segments with different structures and also different chemical composition.

Figure 4 provides examples of particles where the TEM bright field images and EDX analysis reveal some indication of these differences. This apparent transition of the initial crystalline cementite phase to a

Table 1 Steel compositions in wt % (balance Fe)

Steel	C	Si	Mn	P	S	Al	Ni	Cr	Cu	Mo	N
A	0.38	1.82	0.07	nd	nd	1.44	< 0.05	< 0.05	< 0.05	< 0.05	nd
B	0.47	0.22	0.32	nd	nd	< 0.05	1.5	< 0.05	< 0.05	< 0.05	0.009
C	0.50	0.24	0.98	0.011	0.035	0.031	0.14	0.21	0.21	0.03	0.013

nd = not determined

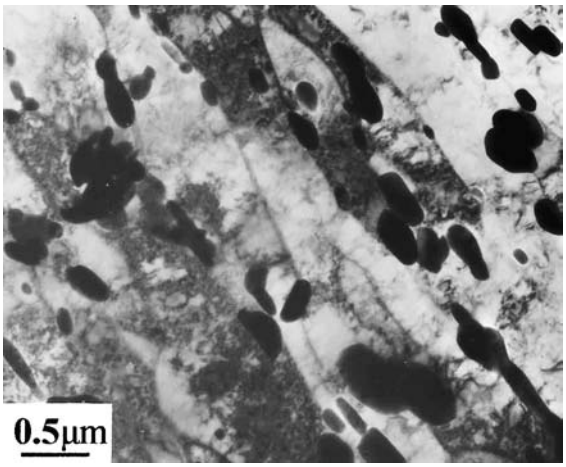

Fig. 1 TEM bright field image illustrating the dispersion of cementite particles, mainly precipitated at the interfaces of ferrite (formerly martensite) laths or plates, after annealing steel A for 0.5 h

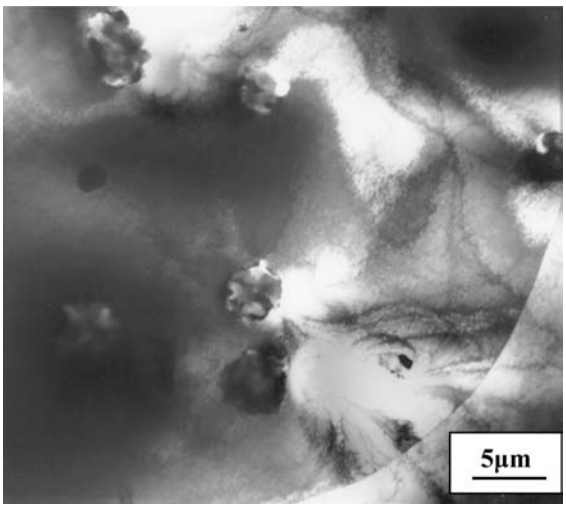

Fig. 2 TEM bright field image showing graphite nodules dispersed within an equiaxed ferrite microstructure after annealing steel A for 1.5 h

partly amorphous particle, during dissolution, was investigated in more detail by EFTEM imaging and PEELS analysis. Figure 5 shows non-quantitative Fe $L_{2,3}$, Mn $L_{2,3}$, O *K*- and C *K*-edge jump ratio images of a complex particle. (These images are obtained by using a ''two-window'' method: an EFTEM image formed by dividing a post-edge image by a pre-edge image, which removes spectral background, shows the qualitative distribution of the element and eliminates the effects of diffraction contrast and, to some extent, specimen thickness.) The major portion of this particle was found to consist of an amorphous phase rich in carbon whilst a smaller part of the particle still remained identifiable as crystalline cementite containing Mn, confirmed by electron diffraction (Fig. 6).

Figure 7 presents EELS spectra of the core loss region of the C *K*-edge (arising from ionisation of carbon 1s electrons to unoccupied 2p electronic states above the Fermi level) from the crystalline portion of two particles, and from the corresponding amorphous regions of the same two particles. For comparison, EELS spectra from a reference cementite precipitate and a graphite nodule in the same steel are also presented. From this comparison it would appear that the position and shape of the C *K*-edge in the EELS spectra changed during annealing. The relative edge onset is lower for the cementite and is typical for a metal carbide. More distinct features are exhibited by the spectra from crystalline cementite, and the relative intensity of the initial electron loss near edge spectroscopy (ELNES) peak is substantially reduced on going from cementite to graphite. (The π^* and σ^* features within the C *K*-edge of amorphous carbon relate to excitation of carbon 1s bonding electrons to unoccupied p states, namely the π and σ antibonding states.) The measured spectra thus indicate that the bonding nature of the carbon in the particles is changing during annealing, from a state similar to that in crystalline cementite to that closer to an amorphous

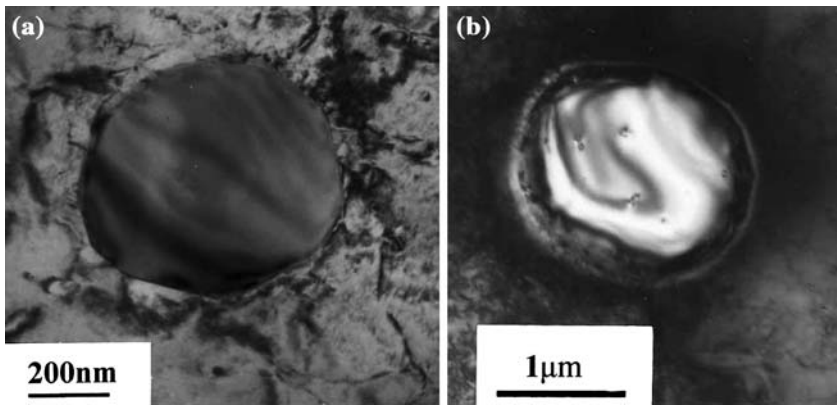

Fig. 3 TEM bright field images of cementite particles stabilised by Mn and Cr after longer term annealing: (**a**) cementite containing ~2 at% Mn in steel B after 50 h, and (**b**) cementite containing ~7 at% Mn and ~3 at% Cr after 1,350 h in steel C

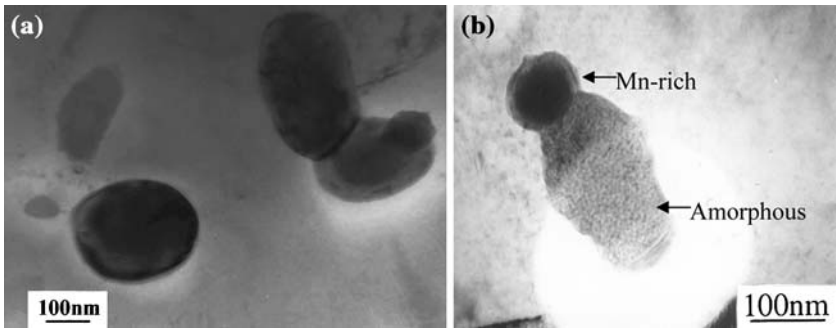

Fig. 4 TEM bright field images of surviving complex particles, after annealing steel A for (**a**) 50 and (**b**) 58 min, respectively [In (**b**) a Mn-rich cementite part and an amorphous carbon-rich part are indicated, as identified by EDX and electron diffraction, respectively. Cementite, amorphous and mixed complex particles are present in (**a**).]

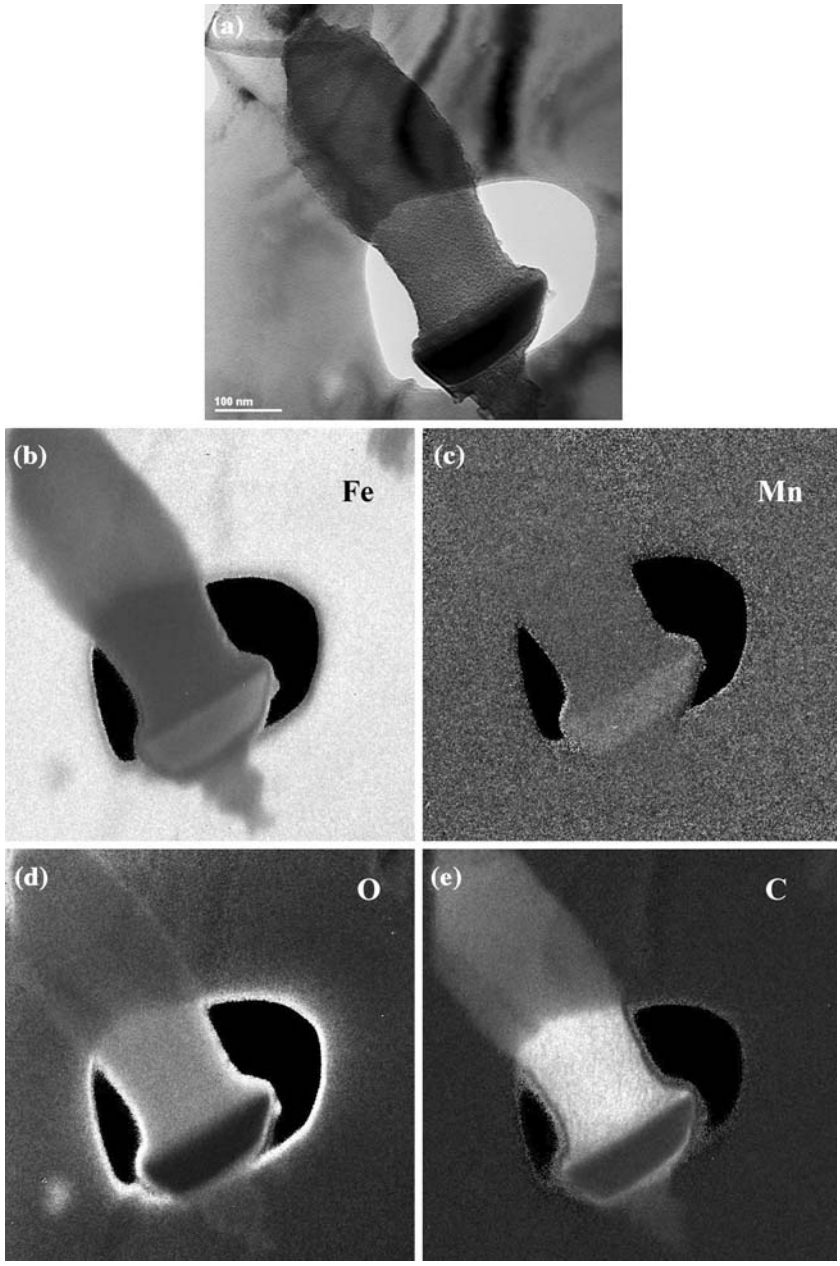

Fig. 5 EFTEM jump ratio images showing a surviving particle in dissolution after annealing steel A for 58 min: (**a**)TEM bright field image; (**b**) Fe $L_{2,3}$-jump ratio image; (**c**) Mn $L_{2,3}$-jump ratio image; (**d**) O *K*-jump ratio image; (**e**) C *K*-jump ratio image

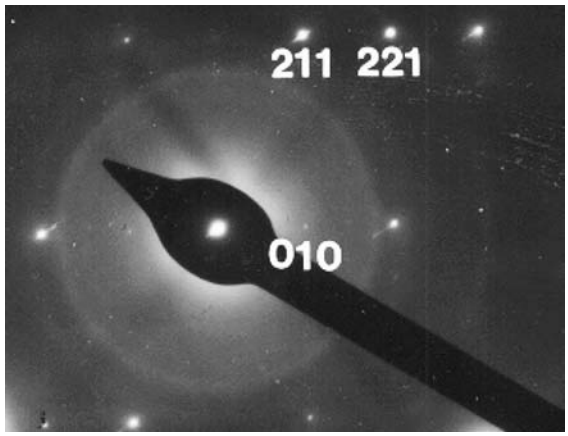

Fig. 6 Electron diffraction pattern from the cementite portion of the complex particle shown in Fig. 4 [The pattern has been indexed to cementite with the [1 0 2] crystal axis parallel to the electron beam.]

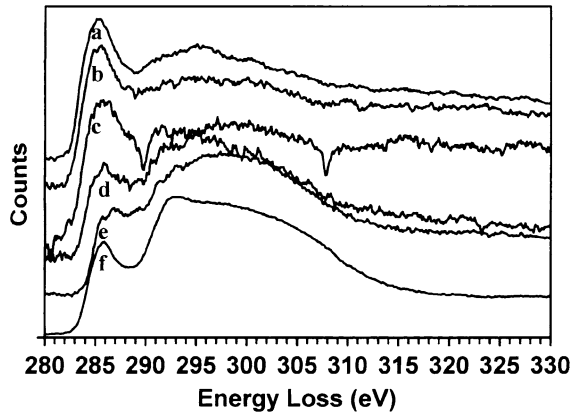

Fig. 7 PEELS spectra of carbon *K*-edges from reference phases and two complex particles in steel A [**a**—from reference cementite; **b**—from cementite part of complex particle 1; **c**—from cementite part of complex particle 2; **d**—from amorphous part of complex particle 1; **e**—from amorphous part of complex particle 2; **f**—from reference graphite formed by annealing at 680 °C.]

carbon structure. Quantitative EELS analysis of the C/Fe ratio from the different parts in a complex particle showed that carbon content increased substantially from around 30 at% for a cementite region (in agreement with the Fe_3C stoichiometry) to around 70 at% for the amorphous part.

EDX analysis of a number of particles in steel A, after annealing times of 0.78 and 0.97 h, respectively, including those containing an identifiable cementite part within a complex particle, showed that they contained an average Mn content of around 2 at%, which is much higher than that of the average concentration of Mn in the cementite particles after 0.5 h, which was found to be less than 0.3 at%. However, a significant variation in the Mn content of cementite particles after 0.5 h annealing was revealed by EDX analysis, as shown in Table 2.

From the data in Table 2 it is clear that the Mn content in the majority of cementite particles was very low, although a small fraction of them had Mn contents as high as ~1.6 at%. This variation in Mn concentration would be expected to have a strong effect on the decomposition of the individual cementite particles during annealing, because Mn is known to increase the stability of cementite [23].

Furthermore, it was also observed, as evident from the bright-field micrograph of Fig. 1 that many cementite particles are not uniformly dispersed as single particles but are frequently clustered together in groups. EDX analysis of some closely spaced cementite particles found that there could still be a significant difference in the Mn content within clusters, as recorded in Table 3.

Discussion

The observations made by analytical transmission electron microscopy have suggested that one mechanism whereby cementite dissolution during a graphitisation anneal of the key experimental steel (steel A) may proceed is by a partial decomposition of the initially crystalline cementite phase to an amorphous state. This proposal is supported by a recent report of the amorphisation of cementite: this was found in high-carbon pearlitic steels that had undergone heavy deformation by cold drawing to wire [24]. It is also known that graphite can nucleate on cementite during the corrosion of iron in strongly carburising atmospheres, known as ''metal dusting'' [25], and it has further been suggested that this occurs by a mechanism in which the graphite grows into the cementite [26]. In addition, evidence for the dissolution of cementite during an austenitisation treatment by the migration of an austenite interface, even of a Widmanstatten form due to the instability caused by concentration gradients within it, has been reported [27]. An alternative description from the present observations might be that the carbon-rich amorphous phase precipitates on

Table 2 Distribution of the Mn content (at%) in cementite particles measured by EDX analysis, in samples from steel A annealed for 0.5 h

Mn (at%)	< 0.1	0.1–0.5	0.5–1.0	1.0–1.6
Number of particles	16	3	5	2
Frequency (%)	61.5	11.5	19.2	7.7

Table 3 EDX analysis of the Mn content (at%) in pairs of closely adjacent cementite particles, in samples from steel A annealed for 0.5 h

Pair	1		2		3		4		5		6		7	
Mn (%)	0.0	0.19	0.15	0.53	0.23	0.64	0.0	0.56	0.0	0.77	0.0	1.07	0.0	1.57

the cementite interfaces during the early stages of annealing. Whichever mechanism is operative it is a strong possibility that these transitional carbon-rich amorphous particles could become nuclei for graphite nodules i.e. a carbon-rich particle from which a more fully graphitised nodule could develop. This infers that the cementite dispersion will be important to the eventual dispersion of graphite nodules.

In the present instance it is proposed that the transitional amorphous state could have been induced by the alloy concentrations in the key experimental steel (steel A). The relatively high concentrations of Si and Al were expected to favour graphite formation, whilst the deliberately low Mn concentration was intended to diminish cementite stability in the steel. These would be the conditions likely to promote an in-situ transformation although this cannot be unambiguously proven from the observations. In steels with more conventional levels of alloying additions (e.g. steels B and C) cementite is very stable, as evidenced by Fig. 3.

There was some evidence that the Mn concentration in some cementite particles in experimental steel A was very low, although it is not entirely clear why there was such a variation in the Mn concentration between particles, even those closely spaced, given that they would have been expected to form and coarsen under similar conditions in the quenched martensite. However, this observation may provide a possible reason for the formation and even the morphology of complex particles, apparently consisting of an identifiable crystalline cementite part and a more amorphous part. This might be that they originated from two closely spaced particles growing together during coarsening, one stabilised by a relatively high Mn content and one containing virtually no Mn that transformed in-situ, or dissolved more rapidly after formation of an adjacent amorphous phase.

However, an equally plausible explanation is that the complex particles arise from formation of the amorphous phase at the cementite particle interface, with rapid growth causing the original shrinking cementite particle to become virtually encased, as observed. The rapidly dissolving cementite would provide a high concentration of carbon at its interface creating favourable conditions for interfacial nucleation of the transitional carbon-rich amorphous phase. Alternatively, the amorphous phase might grow into the dissolving cementite via the migration of an interface.

Elements such as Ca, O and Fe were also found present in EELS spectra from the carbon-rich amorphous particles. However, the Ca content was substantially reduced by plasma cleaning the specimen for 15 min. This means that the presence of Ca is most likely to be due to sample preparation, possibly surface contamination during electrolytic jet polishing. A certain degree of oxidation of the iron matrix always occurs during electropolishing, and so Fe and O are probably the result of iron oxide formation on the surface of the particles as high-resolution TEM imaging revealed very fine crystallites associated with the amorphous part, and electron diffraction confirmed the existence of Fe_3O_4. However, with the same TEM sample preparation procedure, no serious oxidation of iron was found on Cr- and Mn-stabilised cementite particles in Cr and Mn bearing steels, even after more than 1,000 h of annealing at 680 °C, suggesting that a dissolving cementite particle might be less resistant to oxidation during sample preparation than a stable particle.

Conclusions

Analytical transmission electron microscopy has provided evidence of a transitional carbon-rich amorphous phase, associated with decomposing iron carbide cementite particles during a graphitisation anneal of an experimental carbon steel. Large variations in Mn concentration between cementite particles indicated that some particles may be destabilised by a low Mn concentration, and that coupled with the presence of relatively high Si and Al graphitising elements, this could cause these particles to decompose rapidly to supply carbon to the amorphous phase which most probably nucleates at the cementite interface. The formation of this carbon-rich amorphous phase is likely to be an intermediate stage in the graphitisation process.

Acknowledgement This work was initially funded by EPSRC Grant Reference GR/M33693 and continued with part funding from EPSRC Grant Reference GR/R95708.

References

1. Zackay VF, Aaronson HI (eds) (1962) Decomposition of austenite by diffusional processes. Interscience Publishers, New York
2. Speich GR, Clark JB (eds) (1965) Precipitation from iron-base alloys. Gordon and Breach
3. Marder AR, Goldstein JI (eds) (1984) Phase transformations in ferrous alloys. TMS-AIME, Warrendale, PA
4. Sinha AK (1989) Ferrous physical metallurgy. Butterworth
5. Honeycombe RWK, Bhadeshia HKDH (1995) Steels: Microstructure and properties, 2nd edn. Edward Arnold
6. Austin CR, Fetzer MC (1945) Trans ASM 35:485
7. Hickley RH, Quarrell AG (1954) J Iron Steel Inst 178:337
8. Egerton RF (1986) Electron energy loss spectroscopy in the electron microscope. Plenum Press, New York, London
9. Hunt JA, Williams DB (1991) Ultramicroscopy 38:47
10. Brydson R (1991) EMSA Bull 21:57
11. Disko MM, Ahn CC, Fultz B (eds) (1992) Transmission EELS in materials science. TMS, Warrendale, PA
12. Fromm I, Reimer L, Rennekamp R (1992) J Microscopy 166:257
13. Krivanek OL, Gubbens AJ, Delby N, Meyer CE (1992) Microscop Microanal Microstruct 3:187
14. Reimer L (1998) Mater Trans 39:873
15. Fink J, Muller-Heinzerling TH, Pfluger J, Bubenzer A, Koidl P, Crecelius G (1983) Solid State Comm 47:687
16. Fink J, Muller-Heinzerling TH, Pfluger J, Scheerer B, Dischler B, Koidl P, Bubenzer A (1984) Phys Rev B 30:4713
17. Laffont L, Monthioux M, Serin V (2002) Carbon 40:767
18. Berger SD, Mckenzie DR (1988) Phil Mag Lett 57:285
19. Batson PE (1993) Phys Rev B 48:2608
20. McCulloch DG, Brydson R (1996) J Phys Cond Matter 8:3835
21. Daniels HR (2003) PhD Thesis. University of Leeds
22. Daniels HR, Brydson R, Brown A, Rand R (2003) Ultramicroscopy 96:547
23. Goldsmicht HJ (1967) Interstitial alloys. Butterworth, London
24. Nagao M, Makii K, Yaguchi H, Ibaraki N (2001) International symposium on ultrafine grained steels, Fukuoka, Japan, 20–22 Sept. 2001. Iron and Steel Institute of Japan, pp 168–171
25. Grabke HJ, Moszynski D, Muller-Lorenz EM, Schneider A (2002) Surf Interface Anal 34:369
26. Pippel E, Waltersdorf J, Grabke HJ, Strauss S (1995) Steel Res 66:217
27. Liu Z-K, Agren J (1991) Metall Trans 22A:1753